

Unconventional superconductivity in Cr-based nitride $La_3Cr_{10-x}N_{11}$

M Y Zou(邹牧远), J C Jiao(焦嘉琛), K W Chen(陈锴文), C Y Jiang(姜程予), C S Chen(陈长胜), X Li(李鑫), Q Wu(吴琼), N Y Zhang(张宁远), O O Bernal, P C Ho, A Koda, D E MacLaughlin, and L Shu(攻蕾)

Citation: Chin. Phys. B, 2025, 34 (**11**): 117104. DOI: 10.1088/1674-1056/ae001a
http://cpb.iphy.ac.cn; http://iopscience.iop.org/cpb

What follows is a list of articles you may be interested in

Single crystal growth and electronic structure of Fe-doped $Sr_3Ir_2O_7$

Muhammad Waqas, Bingqian Wang(王冰倩), Shuting Peng(彭舒婷), Jianchang Shen(沈建昌), Linwei Huai(淮琳崴), Xiupeng Sun(孙秀鹏), Yu Miao(缪宇), Pelda Uzun, Runqing Luan(栾润青), Zikun Feng(冯梓琨), Dai Pan(潘岱), Xinru Yong(勇欣茹), Hongxu Sun(孙鸿绪), Zhipeng Ou(欧志鹏), and Junfeng He(何俊峰)

Chin. Phys. B, 2025, 34 (**10**): 107101. DOI: 10.1088/1674-1056/adda0b

Ab initio prediction of ground-state magnetic ordering and high-pressure magnetic phase transition of uranium mononitride

Jing-Jing Zheng(郑晶晶), Yuxi Chen(陈禹西), Chengxiang Zhao(赵承祥), Junfeng Zhang(张均锋), Ping Zhang(张平), Bao-Tian Wang(王保田), and Jiang-Jiang Ma(马江将)

Chin. Phys. B, 2025, 34 (**8**): 087101. DOI: 10.1088/1674-1056/add4e6

Interacting Dirac semi-metal state in nonsymmorphic Kondo-lattice compound $CeAgSb_2$

Da-Liang Guo(郭达良), and Huan Li(黎欢)

Chin. Phys. B, 2025, 34 (**6**): 067102. DOI: 10.1088/1674-1056/adc6f6

Possible nodeless $s^{\pm}$-wave superconductivity in twisted bilayer graphene

Zhe Liu(刘哲), Yu Li(李宇), Yi-Feng Yang(杨义峰)

Chin. Phys. B, 2019, 28 (**7**): 077103. DOI: 10.1088/1674-1056/28/7/077103

Heavy fermions in high magnetic fields

M Smidman, B Shen(沈斌), C Y Guo(郭春煜), L Jiao(焦琳), X Lu(路欣), H Q Yuan(袁辉球)

Chin. Phys. B, 2019, 28 (**1**): 017106. DOI: 10.1088/1674-1056/28/1/017106

RAPID COMMUNICATION

Unconventional superconductivity in Cr-based nitride $La_3Cr_{10-x}N_{11}$

M Y Zou(邹牧远)[1], J C Jiao(焦嘉琛)[1], K W Chen(陈锴文)[1], C Y Jiang(姜程予)[1], C S Chen(陈长胜)[1], X Li(李鑫)[1], Q Wu(吴琼)[1], N Y Zhang(张宁远)[1], O O Bernal[2], P C Ho[3], A Koda[4,5], D E MacLaughlin[6], and L Shu(殳蕾)[1,7,†]

[1] *State Key Laboratory of Surface Physics, Department of Physics, Fudan University, Shanghai* 200433, *China*
[2] *Department of Physics and Astronomy, California State University, Los Angeles, California* 90032, *USA*
[3] *Department of Physics, California State University, Fresno, California* 93740, *USA*
[4] *Muon Science Laboratory and Condensed Matter Research Center, Institute of Materials Structure Science, High Energy Accelerator Research Organization (KEK), Tsukuba, Ibaraki* 305-0801, *Japan*
[5] *Department of Materials Structure Science, The Graduate University for Advanced Studies (Sokendai), Tsukuba, Ibaraki* 305-0801, *Japan*
[6] *Department of Physics and Astronomy, University of California, Riverside, California* 92521, *USA*
[7] *Shanghai Research Center for Quantum Sciences, Shanghai* 201315, *China*

(Received 5 July 2025; revised manuscript received 10 August 2025; accepted manuscript online 28 August 2025)

Magnetization, specific heat, and muon spin relaxation (μSR) experiments have been carried out on the Cr-based nitride superconductor $La_3Cr_{10-x}N_{11}$, which exhibits a number of unconventional superconducting properties. The susceptibility $\chi(T)$ shows nearly perfect superconducting diamagnetism ($4\pi\chi(T=0)\approx -1$) and a remarkably high upper critical field $\mu_0 H_{c2} = 11.2$ T. The specific heat displays activated exponential behavior $\exp(-\Delta_0/k_B T)$, together with a large and field-dependent residual Sommerfeld coefficient. Transverse-field muon spin relaxation (μSR) measurements suggest s+s-wave or p-wave pairing symmetry, ruling out single s-wave pairing. Zero-field μSR yields no statistically significant evidence for time reversal symmetry breaking (TRSB), and places an upper bound of 1.5(1.3) ms^{-1} on any TRSB-induced muon relaxation rate at $T = 0$. Our results suggest that the unconventional superconductivity in $Ln_3Cr_{10-x}N_{11}$, Ln = La and Pr, is mainly due to Cr 3d electrons and is similar in both compounds, whereas Pr 4f electrons are primarily responsible for the TRSB superconductivity observed in $Pr_3Cr_{10-x}N_{11}$.

Keywords: muon spin relaxation/rotation, heavy fermion superconductor, chromium-based superconductor

PACS: 71.27.+a, 74.70.Tx, 76.75.+i

DOI: 10.1088/1674-1056/ae001a **CSTR:** 32038.14.CPB.ae001a

1. Introduction

Unconventional superconductivity has been an intriguing topic in condensed matter physics for quite some time. Various novel properties, including unconventional pairing symmetry beyond BCS theory,[1–4] competition between superconductivity and density-wave order, and coexistence of superconductivity and magnetism,[5–7] have been observed in unconventional superconductors. Complex phase diagrams with exotic quantum states have been widely studied in heavy fermion, copper-based, and iron-based superconductors since they were first discovered.[8–13] Heavy-fermion systems have received much attention due to the discovery of quantum critical points and spin-triplet superconductivity in recent years.[14–20] However, there are still no general conclusions regarding mechanisms for unconventional superconductivity,[21,22] and in particular the pairing mechanisms require further investigation.

Several Cr-based superconductors have been reported to exhibit unconventional superconductivity. Nuclear magnetic resonance (NMR)[23] and neutron-scattering measurements[22,24] on the superconductor CrAs revealed an antiferromagnetic edge state near T_c, indicating magnetic exchange interactions as a possible superconducting pairing mechanism. In the quasi-one-dimensional superconductor $K_2Cr_3As_3$, the upper critical magnetic field H_{c2} is three times the Pauli paramagnetic limit,[25,26] and the presence of nodes in the superconducting gap was indicated by muon spin relaxation (μSR) experiments.[27,28] $K_2Cr_3As_3$ was suggested to be a candidate material for p-wave pairing symmetry due to strong ferromagnetic spin fluctuations.[29–31] Time-reversal symmetry breaking (TRSB) superconductivity was discovered in the Pr-based filled skutterudite superconductors $PrOs_4Sb_{12}$[18] and $PrPt_4Ge_{12}$.[16] The Pr 4f electrons are considered to play an important role in the unconventional superconductivity of these compounds, since the isomorphic compounds $LaOs_4Sb_{12}$[32] and $LaPt_4Ge_{12}$[33] are conventional superconductors without TRSB.

A Cr-based nitride superconductor $Pr_3Cr_{10-x}N_{11}$ (PCN)

†Corresponding author. E-mail: Leishu@fudan.edu.cn

© 2025 Chinese Physical Society and IOP Publishing Ltd. All rights, including for text and data mining, AI training, and similar technologies, are reserved.

was reported in 2019 ($T_c = 5.25$ K).[34] PCN exhibits a large upper critical field $\mu_0 H_{c2} = 20$–30 T, TRSB in the superconducting state, and possible p-wave pairing symmetry.[35] Intriguingly, the La superconductor isomorph $La_3Cr_{10-x}N_{11}$ (LCN), $T_c = 4.6$ K,[36] also has a large $\mu_0 H_{c2} = 12.2$ T, which may indicate unconventional superconductivity in it as well. Electronic structure calculations[34,36] conclude that the dominant electron density of states at the Fermi surface arises from Cr 3d electrons in both LCN and PCN. These results immediately raise the question of the origin of the unconventional superconductivity in both compounds. A detailed study of the superconductivity of LCN, especially concerning time-reversal symmetry, is clearly needed.

The muon spin rotation/relaxation (μSR) technique uses the muon spin as a probe of magnetic properties on the atomic scale,[37,38] and is a useful technique for exploring novel features of unconventional superconductors.[39] Its high sensitivity to local magnetic fields makes μSR in zero applied field (ZF-μSR) useful to study extremely small internal fields in materials, and in particular to probe TRSB in superconductors.[40,41] The additional relaxation rate in transverse-field (TF-μSR) experiments in the vortex state of a type-II superconductor[42] is due to the field distribution in the vortex lattice, and is associated with the superconducting penetration depth and the superfluid density. Its temperature dependence provides important information on the symmetry of superconducting Cooper pairs.[43,44]

This paper reports the results of dc magnetic susceptibility, resistivity, specific heat, and μSR experiments performed on a polycrystalline sample of LCN. The presence and unusual field dependence of a residual $T = 0$ electronic specific heat coefficient γ_0, the large H_{c2}, and the temperature dependence of the superfluid density are found to be similar to those of PCN, but ZF-μSR results indicate that TRSB is quite unlikely in LCN. We conclude that the unconventional superconductivity is similar in the two compounds, and primarily originates from the Cr 3d electrons. Pr 4f electrons in PCN are apparently responsible for TRSB superconductivity in that compound, but seem to play at most a minor role in superconducting pairing.

2. Experiment

Polycrystalline samples of LCN were prepared by direct reactions of the corresponding binary nitrides, using the procedure of Li *et al.*[36] LaN and a mixture of CrN and Cr_2N with a mass ratio of 3:7 were mixed thoroughly in a glove box filled with Ar gas. The mixed powder was pressed into pellets and sealed in an evacuated quartz tube. The tube was then placed in a muffle furnace to start the sintering process. The temperature was increased to 1000 °C over a day, maintained for 50 hours, and then cooled to room temperature. The sintered pellets were then ground in a glove box. Additional LaN (about 10% of the total mass) was added to react with excess Cr_2N. After thorough mixing, the mixture was again pressed into pellets and sealed in a quartz tube filled with nitrogen to reduce loss during the reaction. The pellets were again sintered, with the temperature increased to 1165 °C at the same rate as in the first sintering. This temperature was maintained for 120 hours to ensure a complete reaction. The temperature was slowly lowered to around 800 °C, and then cooled to room temperature. Since the quartz tube could soften at 1165 °C, the slow cooling helped to ensure its integrity and the stability of the internal nitrogen environment. During the entire process, the time when the sample was exposed to air was kept below two minutes.

Due to limitations in the growth method, impurities and Cr vacancies are inevitably present in the final product. In a previous study,[36] x-ray diffraction measurements on a similarly-prepared LCN sample found a low level of unreacted Cr_2N to be the primary impurity component.

The magnetization of LCN was measured using a Quantum Design MPMS SQUID magnetometer. The temperature dependence of the electrical resistivity $\rho(T)$ was measured in a Quantum Design PPMS using a standard four-probe method. For this measurement, a powder sample was pressed and cut into a rectangle, and annealed silver wires were glued to the sample with conductive silver adhesive. Resistances were measured between 1.8 K and 300 K. The PPMS with a ^{3}He insert was used to measure the specific heat of the sample between 400 mK and 300 K.

The μSR experiments were performed on the DR spectrometer at the M15 beam line, TRIUMF, Vancouver, Canada, and the S1 ARTEMIS spectrometer at J-PARC, Ibaraki, Japan. Pellets of LCN were attached to high-purity Ag sample holders using diluted GE varnish. Experiments were carried out down to 100 mK. μSR data were analyzed using the `musrfit` software package.[45]

3. Results

3.1. Susceptibility and magnetization

Figure 1(a) shows the temperature dependence of the dc magnetic susceptibility χ of LCN from 1.9 K to 7 K in a magnetic field $\mu_0 H = 2$ mT, for both zero-field cooling (ZFC) and field cooling (FC). The superconducting diamagnetism is ∼70% larger than previously reported,[36] and approaches the full shielding value $4\pi\chi = -1$ at low temperatures. This is evidence that the impurity content of the sample is small and the sample is a bulk superconductor. From the magnetic field dependence of χ at different temperatures, shown in Fig. 1(b), the lower critical field $\mu_0 H_{c1}$ is estimated to be about 10 mT.

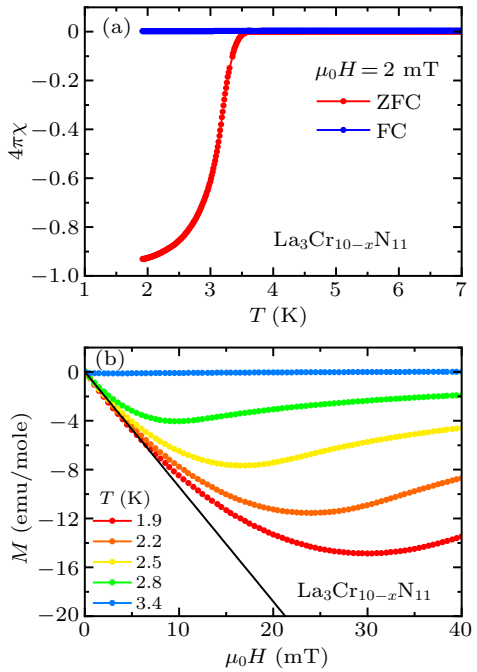


Fig. 1. (a) ZFC and FC temperature dependence of dc magnetic susceptibility χ of LCN, $\mu_0 H = 2$ mT. (b) Field dependence of dc magnetization M. Black line: fit of H_{c1}.

3.2. Electrical resistivity

The temperature dependence of the zero-field electrical resistivity ρ of LCN, shown in Fig. 2(a), exhibits typical metallic behavior above T_c. The onset of superconductivity at zero field is 4.0 K, and the resistivity reaches zero at 3.6 K. The inset shows the field dependence of the superconducting transition.

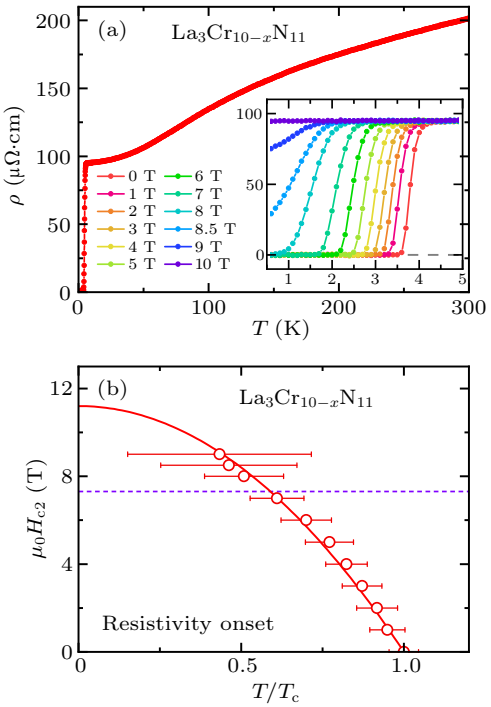


Fig. 2. (a) Temperature dependence of electrical resistivity ρ for LCN at zero field. Inset: transitions measured at different applied magnetic fields. (b) Upper critical field H_{c2} obtained from dc resistivity measurements. The "error bars" are transition widths. Curve: fit of Eq. (1) to the data. Dashed line: Pauli paramagnetic limit.

Figure 2(b) shows the temperature dependence of H_{c2} from the resistivity measurements. The data can be fit by the empirical formula[34,36]

$$H_{c2}(T) = H_{c2}(0)(1-t^2), \tag{1}$$

where $t = T/T_c$. The fit value of $\mu_0 H_{c2}(0)$ is 11.2(2) T, lower than that for PCN (20–30 T),[35] but significantly higher than the Pauli paramagnetic limit $\mu_0 H_P = 1.84 T_c = 7.4$ T.[26] This suggests that LCN is also a candidate unconventional superconductor.

3.3. Specific heat

The specific heat $C(H,T)$ of LCN was measured for applied fields in the range 0–9 T. The temperature dependence of C/T in zero field is shown in Fig. 3(a). The usual relation $C/T = \gamma_n + \beta T^2$[46] for normal-state electronic and phonon contributions in a metal is a good fit to the data above T_c, yielding $\gamma_n = 0.170(1)4$ mJ·g^{-1}·K^{-2} = 185(1) mJ·mol^{-1}·K^{-2} and $\beta = 0.41(1)$ J·g^{-1}·K^{-4}. The large value of γ_n is similar to that of PCN,[35] indicating strong electron correlations. For comparison, γ (Cr_2N) = 22 mJ·mol^{-1}·K^2.[34]

The electronic specific heat C_e was obtained by subtracting the βT^3 phonon contribution. Figure 3(b) shows the temperature and field dependencies of $C_e/\gamma_n T$ below 5 K. Sharp superconducting transition jumps are observed, which shift to lower temperatures and are suppressed by applied field. The increase ΔC_e of C_e at T_c in zero field yields a ratio $\Delta C_e/\gamma_n T_c = 0.715(4)$. A field-dependent residual specific heat coefficient $(C_e/\gamma_n T)_{T\to 0}$ is observed. This was also seen in PCN,[34,35] and attributed[34] to a Cr_2N impurity phase. The normal-state specific heats per unit mass of LCN/PCN and Cr_2N are similar, however, so that an impurity-phase scenario would require a Cr_2N impurity mass comparable to that of LCN or PCN. The very small impurity x-ray reflections in both LCN[36] and PCN[34] make this unlikely. Furthermore, γ_0 is strongly field-dependent in LCN [Fig. 3(b)], which would not be expected for an impurity phase. A similar field dependence is observed in PCN.[35]

The curves in Fig. 3(b) are fits of the data to the sum of the full-gap superconducting model $C_e/T \propto e^{-\Delta_0/k_B T}$ [47,48] and a constant $\gamma_0(H)$, with entropy balance imposed between the superconducting and normal states. For $H = 0$ $\gamma_0(0)/\gamma_n \approx 0.5$ and $\Delta_0 = 0.281(6)$ meV, $\Delta_0/k_B T_c = 0.91(2)$. These are comparable to the values for PCN.[35]

The temperature dependence of H_{c2} determined from the specific heat jumps, shown in Fig. 3(c), is consistent with the results from the resistivity measurements [Fig. 2(b)]. From a fit of Eq. (1) to the data, $\mu_0 H_{c2}(0) = 10.9(2)$ T, which is within experimental error the same as the result 11.2(2) T from resistivity measurements.

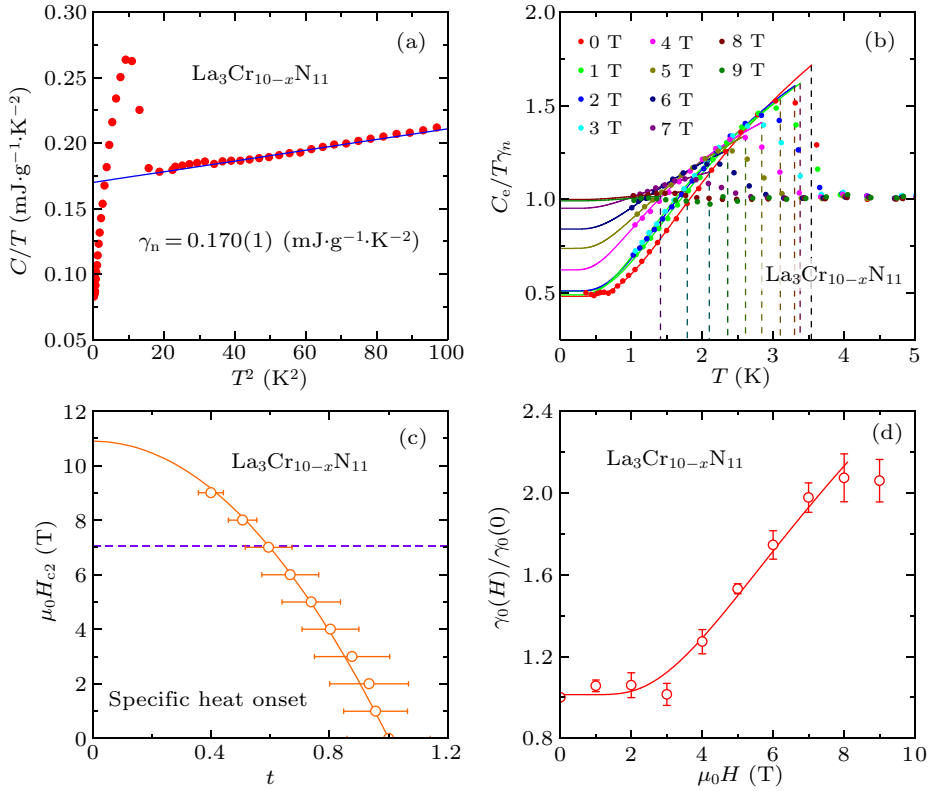


Fig. 3. (a) Temperature dependence of C/T at zero field. Line: fit of $C/T = \gamma + \beta T^2$ to the normal-state data. (b) Temperature and field dependence of relative electronic specific heat $C_e/\gamma_n T$. Curves: fits of the full-gap model $C_e/T \propto e^{-\Delta_0/k_B T}$ [47,48] and a residual constant (see text). Vertical dashed lines: superconducting transition temperatures. (c) Temperature dependence of the upper critical field H_{c2}. Curve: fit of Eq. (1) to the data. Dashed line: Pauli paramagnetic limit. (d) Field dependence of relative residual specific heat coefficient $\gamma_0(H)/\gamma_0(0)$. Curve: fit of Eq. (2) to the data.

Figure 3(d) shows the field dependence of γ_0. The empirical formula

$$[\gamma_0(H) - \gamma_0(0)]/\gamma_n = e^{-H^*/H}, \tag{2}$$

which was used for PCN,[35] also describes $\gamma_0(H)$ for LCN up to $\mu_0 H \approx 8$ T [curve in Fig. 3(d)]. Above this field, $\gamma_0(H)$ seems to saturate, resembling the behavior in the ferromagnetic superconductors UTe_2 [49] and URhGe.[50]

3.4. TF-μSR

The μSR asymmetry spectrum $A(t)$ is the sum of a contribution $A_s(t)$ from muons that stop in the sample and a "background" contribution $A_b(t)$ from muons that stop in the silver sample holder. The TF-μSR asymmetry data are well described by[44]

$$A(t) = A_s(t) + A_b(t), \quad \text{with} \tag{3}$$

$$A_s(t) = A_{s0} \exp\left(-\tfrac{1}{2}\sigma_s^2 t^2\right) \cos(\gamma_\mu B_s t + \phi), \tag{4}$$

$$A_b(t) = A_{b0} \exp\left(-\tfrac{1}{2}\sigma_b^2 t^2\right) \cos(\gamma_\mu B_b t + \phi), \tag{5}$$

where σ_s and σ_b are the corresponding relaxation rates and γ_μ is the muon gyromagnetic ratio. Gaussian relaxation is assumed.

Equations (3)–(5) were fit to the TF-μSR data. The background rate σ_b was negligibly small, and the phase ϕ and B_b were constant. Equation (5) with the resulting background parameters was then subtracted from the data to yield the experimental $A_s(t)$. Figure 4(a) shows representative results in the normal state and superconducting vortex-lattice state of LCN, applied field $\mu_0 H = 40$ mT. For clarity, the data are shown in a reference frame rotating[51] at a frequency corresponding to a field of 35 mT. It can be seen that the damping of the signal is enhanced in the superconducting state.

In the normal state, the sample rate σ_s is due to host nuclear dipolar fields and is independent of temperature. In the vortex state of a type-II superconductor, σ_s is enhanced by the flux-line lattice (FLL) field distribution $n(B)$,[42] and increases with decreasing temperature below T_c. The internal field distribution is a convolution of $n(B)$ and the nuclear dipole field distribution, so that the observed σ_s is given by

$$\sigma_s = \sqrt{\sigma_{sc}^2 + \sigma_n^2}, \tag{6}$$

where σ_{sc} is the rate in the Gaussian approximation for $n(B)$.[52]

The temperature dependence of σ_{sc} obtained using Eq. (6) and $\sigma_n = 0.301(7)$ μs^{-1} is shown in Fig. 4(b). The temperature dependence of σ_s itself is shown in the inset. The increase is evidence for bulk superconductivity, although by itself it does not indicate a low level of normal-state regions in the sample. If present, these reduce the amount of superconduct-

ing sample and result in a smaller observed increase.

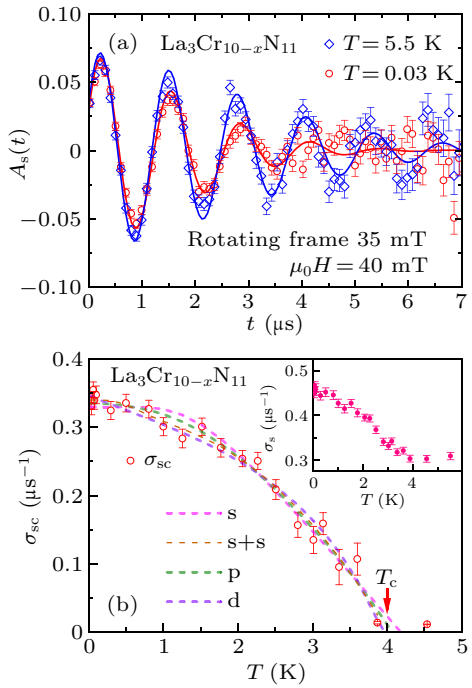


Fig. 4. (a) Representative TF-μSR asymmetry spectra $A(t)$ from LCN in the normal (diamonds) and superconducting (circles) states, $\mu_0 H = 40$ mT. Curves: Eq. (4) (see text). (b) Temperature dependence of superconducting relaxation rate σ_{sc} [Eq. (6)]. Curves: fits of Eq. (9) to the data with four pairing symmetries as indicated. Inset: temperature dependence of measured sample rate σ_s.

In general

$$\sigma_{sc} = \gamma_\mu [\overline{(\Delta B)^2}]^{1/2}, \tag{7}$$

where $[\overline{(\Delta B)^2}]^{1/2}$ is the rms width of $n(B)$. For an isotropic extreme type-II superconductor,[53]

$$\overline{(\Delta B)^2} = 0.00371 \Phi_0^2 \lambda_L^{-4}, \tag{8}$$

where $\Phi_0 = 2.07 \times 10^{-15}$ Wb is the flux quantum. The London penetration depth λ_L is related to the density n_s of superconducting carriers and m^* by the London equation $1/\lambda_L^2 = 4\pi n_s e^2/m^* c^2$.[46] Thus $\sigma_{sc} \propto n_s$.

For a spherical Fermi surface, the temperature dependence of $\sigma_s(T)/\sigma_s(0)$ can be written as[15,54,55]

$$\begin{aligned} \frac{\sigma_{sc}(T)}{\sigma_{sc}(0)} &= \frac{n_s(T)}{n_s(0)} \\ &= 1 + \frac{1}{2\pi} \int_0^{2\pi} \int_0^{\pi} \int_\Delta^\infty \mathrm{d}E \sin\theta \,\mathrm{d}\theta \,\mathrm{d}\phi \\ &\quad \times \frac{\mathrm{d}f}{\mathrm{d}E} \frac{E}{\sqrt{E^2 - \Delta^2}}, \end{aligned} \tag{9}$$

where $n_s(0)$ is the superfluid density at zero temperature, E is the quasiparticle energy relative to E_F, $f(E)$ is the Fermi function,

$$\Delta = \Delta(T, \phi, \theta) = \Delta_0 \delta(T/T_c) g(\phi, \theta), \tag{10}$$

$$\delta(T/T_c) = \tanh\{1.82[1.018(T_c/T - 1)]^{0.51}\}, \tag{11}$$

where Δ_0 is the $T = 0$ superconducting energy gap, $\delta(T/T_c)$ is the gap function,[56] and $g(\phi, \theta)$ is the angular dependence of the gap.

Fits of Eq. (9) to the $\sigma_{sc}(T)$ data for angular dependencies corresponding to four gap symmetries are plotted in Fig. 4(b). The fitting parameters are listed in Table 1.

Table 1. Gap functions and fitting parameters for gap symmetry models.

Model	s	s+s	p	d
$g(\phi,\theta)$	1	1	$\lvert\sin(\theta)\rvert$	$\lvert\cos(2\phi)\rvert$
Nodes	none	none	point	line
$\sigma_s(0)$ (μs^{-1})	0.330(6)	0.341(7)	0.336(5)	0.346(5)
T_c (K)	4.17(15)	4.06(10)	4.07(11)	3.94(5)
Δ_0 (meV)	0.56(3)	0.65(5) (85%)	0.74(4)	0.99(2)
		0.14(8) (15%)		
$\Delta_0/k_B T_c$	1.55(8)	1.86(14)	2.11(10)	2.94(6)
		0.41(24)		
Statistical χ^2	1.48	0.96	1.01	1.04

The statistical χ^2 is large for the s-wave model, but satisfactory for the others. The d-wave model, however, has a strongly nonzero negative slope at $T = 0$, whereas the data favor a smaller or zero slope; the weaker nonzero slope of the p-wave model could be hidden in the uncertainty. We conclude that the s+s-wave and p-wave models are the most likely candidates for the superfluid symmetry of LCN.

For all models $\sigma_{sc}(0) \approx 0.34\ \mu s^{-1}$, which from Eqs. (7) and (8) yields $\lambda_L \approx 550$ nm. This large penetration depth is in agreement with observation of a large residual specific heat term γ_0 (Subsection 3.3). As noted above, however, normal-state inclusions in the sample would make the observed value of $\sigma_{sc}(0)$ a lower bound, so that λ_L could be smaller than this estimate. Fit values of T_c range around 4.0 K, somewhat higher than the value of 3.6 K from the ZFC susceptibility [Fig. 1(a)].

3.5. ZF- and LF-μSR

The ZF-μSR is sensitive to small local magnetic fields (~0.01 mT).[57,58,60] The observed onset of small fields below T_c in PCN,[35] which was attributed to TRSB, motivated our ZF-μSR study of LCN. ZF-μSR spectra at 0.3 K ($T < T_c$) and 5.5 K ($T > T_c$), obtained at the J-PARC ARTEMIS spectrometer, are shown in Fig. 5(a). The data are well fit by a single exponential and a non-relaxing background

$$A(t) = A_s e^{-\Lambda t} + A_b. \tag{12}$$

There is very little difference between the two spectra.

Static and dynamic field contributions to the muon spin relaxation rate are hard to distinguish at zero field.[37,38] Longitudinal-field (LF) μSR experiments were also carried out, in which a magnetic field H_L was applied parallel to the initial muon spin polarization. A large enough applied field

"decouples" static local fields from the muon spin polarization, and any remaining relaxation is dynamic in origin. Representative normal-state LF-μSR results, obtained at the TRIUMF DR spectrometer, are shown in Fig. 5(b). An applied field of 5 mT is sufficient to almost completely decouple the static relaxation. This indicates that the observed ZF relaxation rates are dominated by a static field distribution, the source of which is likely ^{139}La and ^{14}N nuclear dipoles.

The temperature dependence of the ZF rate Λ is shown in Fig. 5(c). In PCN, $\Lambda(T)$ increases more or less linearly below T_c,[35] so that two linear segments with continuity at T_c,

$$\Lambda(T) = \begin{cases} \Lambda_n, \ T > T_c \quad \text{(average)}, \\ \Lambda_n + \Lambda_{sc}(0)(1 - T/T_c), \ \ T < T_c, \end{cases} \tag{13}$$

were fit to the LCN data. A more detailed fit function such as that used by Chen *et al*. is not warranted by the statistics.

The dashed green line in Fig. 5(c) gives the "hypothetical TRSB" of Eq. (13) to the LCN data, and the average of all points is shown by the dashed red line. The results and statistical parameters are given in Table 2. The reduced χ^2_{red} is good for both fits. The confidence level is the probability that a random repeat of the given experiment would observe a worse χ^2.[61]

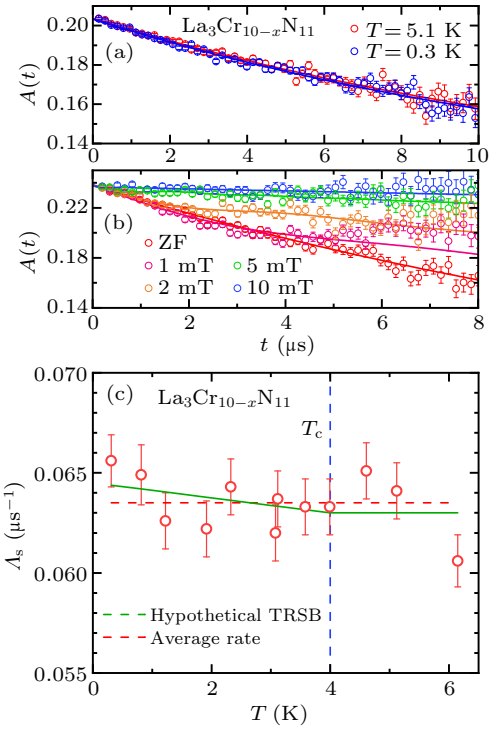


Fig. 5. (a) ZF-μSR asymmetry spectra at 0.3 K and 5.5 K. Curves: fits of Eq. (12) to the data. (b) Field dependence of LF-μSR asymmetry spectra, $T = 4.037$ K. Curves: fits to LF relaxation functions for intermediate fields.[59] (c) Temperature dependence of ZF-μSR relaxation rate $\Lambda(T)$. Green dashed lines: average above superconducting T_c and linear fit below T_c (hypothetical TRSB, see text). Red dashed dashed line: average over all temperatures. Vertical dashed line: T_c from susceptibility and resistivity measurements (Subsection 3.1).

Table 2. ZF-μSR: Linear fit parameters and statistics.

Parameter	$\Lambda_{sc}(0)$	Λ_n	Λ_{av}	χ^2_{red}	Confidence level
Hypothetical TRSB	0.0015(13)	0.0630(6)	–	1.044	40.3%
Average	–	–	0.0635(4)	1.076	37.6%

4. Discussion and summary

4.1. Sample quality

The experiments reported here characterize LCN in several aspects, and a number of its properties indicate that it is an unconventional superconductor. The Cr vacancy concentration x is hard to control during synthesis,[62] and the difference between measured values of the transition temperature T_c (4.6 K reported in Ref. [36], 3.6–4.0 K in the present study) may be due to differences in x. Nevertheless, an important result is that the $T = 0$ superconducting diamagnetic susceptibility is close to the value $-1/4\pi$ expected for a bulk superconductor. This indicates high sample quality. In addition, the small and temperature-independent ZF-μSR normal-state relaxation rate [Fig. 5(c)] indicates a negligible level of paramagnetic impurities in the sample.

4.2. Electronic specific heat, normal-state ZF-μSR

LCN exhibits a large normal-state Sommerfeld coefficient $\gamma_n = 185(1)$ mJ·mol^{-1}·K^{-2}, somewhat greater than in a previous report (169 mJ·mol^{-1}·K^{-2}[36]) and similar to the value 207 mJ·mol^{-1}·K^{-2} for PCN.[35] This large term can be attributed to the intrinsic properties of LCN, but is 10 times greater than the theoretical prediction for the contribution from Cr 3d orbitals near the Fermi surface.[34] In PCN the large γ_n value has been linked to Pr 4f spin dynamics.[34,35] But from the normal-state ZF-μSR results (Subsection 3.5), the μSR relaxation in LCN is clearly dominated by the (quasi)static nuclear dipolar field distribution; there is no evidence for the dynamic relaxation that would be associated with fluctuating electronic spins. The similarity of the γ_n values and $T \to 0$ behavior in LCN and PCN also casts doubt on a spin-fluctuation mechanism in PCN. It can be concluded that in both compounds most of the density of states at the Fermi energy comes from Cr 3d orbitals in $Ln_3Cr_{10-x}N_{11}$, in agreement with previous DFT calculations,[34,36] although the measured specific heats are an order of magnitude larger than those predicted by theory.

The temperature dependence of $C_e(T)/T$ in superconducting LCN exhibits the exponential behavior at low temperatures of a fully-gapped superconductor, but this does not

completely resolve the question of superconducting gap nodes. The fit yields a value of $\Delta_0/k_BT_c \sim 0.92$; it and the jump $\Delta C_e(T_c)/\gamma_n T_c = 0.715(1)$ are both considerably smaller than their BCS values (1.76 and 1.43, respectively[54]).

There are at least two candidate scenarios for this reduction: the "erasure" of point gap nodes on the Fermi surface by mixing of states with different orbital angular momenta,[63] and multi-band superconductivity.[56,64] Each of these is consistent with the observed TF-μSR relaxation, for (erased) p-wave and s+s-wave symmetries respectively [Fig. 4(b) and Table 1].

The residual $T = 0$ value of $C_e/\gamma_n T$ [Fig. 3(b)] exhibits an unusual exponential magnetic field dependence [Fig. 3(d)], similar to that observed in PCN,[35] UTe_2,[49] and URhGe,[50] with saturation above ~ 8 T. For UTe_2, several explanations have been discussed,[49,65,66] such as field-induced enhancement of anisotropic gap structures, field-enhanced correlations among unpaired electrons, and Fermi surface instability. The microscopic origin of this behavior in LCN remains an open question.

4.3. Large H_{c2}, TF- and ZF-μSR, superfluid density, time-reversal symmetry

LCN and PCN differ significantly from the comparable filled skutterudite superconductors $LnOs_4Sb_{12}$, Ln = La and Pr. Both PCN and LCN exhibit $H_{c2}(0)$ exceeding the Pauli limit, as does $PrOs_4Sb_{12}$, whereas $LaOs_4Sb_{12}$, unlike LCN, has BCS-like superconducting properties including a considerably smaller $H_{c2}(0)$.[67] In the skutterudites, this difference was attributed to CEF-split 4f levels in the Pr compound. The large H_{c2} in LCN and PCN can be attributed to spin-triplet pairing, multi-band effects, and strong coupling.

The TF-μSR experiment yields the temperature dependence of the superfluid density of LCN, with results similar to those observed in PCN.[35] The TF-μSR results (Subsection 3.4) suggest that s-wave superconducting pairing symmetry is unlikely in LCN; p-wave and s+s-wave pairing are more likely candidate superconducting symmetries. However, unlike PCN, no statistically significant evidence for a spontaneous magnetic field was obtained from ZF-μSR, indicating the probable absence of TRSB. It can be seen [Fig. 5(c), Table 2] that the average and the hypothetical TRSB fits to the relaxation rate data are essentially statistically equivalent. The hypothetical TRSB fit rate $\Lambda_{sc}(T = 0) = 1.5(1.3)$ ms^{-1} is only a few percent of the static background rate [63(1) ms^{-1}] or the TRSB rate for PCN [42(5) ms^{-1} [35]], and differs from zero only by an amount of the order of its standard deviation.

We conclude that $\Lambda_{sc}(T = 0)$ is only an upper bound on any rate due to TRSB in LCN. Comparing LCN with PCN, the unconventional electronic structure and superconductivity exhibited by PCN both remain intact in LCN despite the absence of 4f electrons. This is evidence against their direct role as the primary source of unconventional superconductivity. Pr 4f electrons do, however, induce TRSB in PCN and thus could potentially influence superconducting pairing.

5. Conclusions

This paper reports a comprehensive characterization of normal- and superconducting-state properties of LCN using a number of techniques. Many properties are similar in LCN and isomorphic PCN. In both compounds, the jump $\Delta C_e/T_c$ in the specific heat at the superconducting transition is small, and the critical field $H_{c2}(0)$ exceeds the Pauli limit. Both exhibit a mysterious residual term $\gamma_0(H)$ in the specific heat coefficient with an exponential dependence on applied field. TF-μSR measurements yield similar temperature dependencies of the superfluid density in both compounds that rule out single-band s-wave superconducting pairing symmetry. The principal difference between them is in the results of ZF-μSR experiments, which reveal substantial TRSB relaxation in PCN but only a very low upper bound on it in LCN.

We conclude that, with the exception of TRSB, unconventional superconductivity is remarkably similar in LCN and PCN, a situation that is not found in other rare-earth-based superconductor families. The unconventional superconductivity observed in LCN seems to serve as the basis for that in PCN, with TRSB the only observed effect of Pr 4f electrons in PCN. The 4f electrons influence the superconducting symmetry of PCN but do not seem to provide the basic pairing mechanism. Our experiments motivate further studies of Cr-based superconductors; a full understanding of the role of 4f electrons requires additional experimental investigation.

Acknowledgements

We are grateful to G. D. Morris, B. Hitti, and D. Arsenau of the TRIUMF CMMS and the staff of J-PARC S1 (Experiment No. 2024A0208) for their valuable help during the μSR experiments. This work was funded by the National Key Research and Development Program of China (Grant No. 2022YFA1402203), the National Natural Science Foundations of China (Grant No. 12174065), the Innovation Program for Quantum Science and Technology (Grant No. 2024ZD0300104), and the Shanghai Municipal Science and Technology Major Project (Grant No. 2019SHZDZX01).

References

[1] Emery V J and Kivelson S A 1995 *Nature* **374** 434
[2] Lee P A 1999 *Phys. C* **317–318** 194
[3] Norman M R and Pépin C 2003 *Rep. Prog. Phys.* **66** 1547
[4] Kotliar G and Liu J L 1988 *Phys. Rev. B* **38** 5142
[5] Chen K W , Liu X Q, Jiao J C, Zou M Y, Jiang C Y, Li X, Luo Y X, Wu Q, Zhang N Y, Guo Y F and Shu L 2024 *Phys. Rev. Lett.* **25** 256503
[6] Khim S, Landaeta J F, Banda J, Bannor N, Brando M, Brydon P M R, Hafner D, Küchler R, Cardoso-Gil R, Stockert U, Mackenzie A P, Agterberg D F, Geibel C and Hassinger E 2021 *Science* **373** 1012

[7] Dikin D A, Mehta M, Bark C W, Folkman C M, Eom C B and Chandrasekhar V 2011 *Phys. Rev. Lett.* **107** 056802
[8] Zhang J, Ding Z F, Tan C, Huang K, Bernal O O, Ho P C, Morris G D, Hillier A D, Biswas P K, Cottrell S P, Xiang H, Yao X, MacLaughlin D E and Shu L 2018 *Sci. Adv.* **4** eaao5235
[9] Wu M K, Ashburn J R, Torng C J, Hor P H, Meng R L, Gao L, Huang Z J, Wang Y Q and Chu C W 1987 *Phys. Rev. Lett.* **58** 908
[10] Maeda H, Tanaka Y, Fukutomi M and Asano T 1988 *Jpn. J. Appl. Phys.* **27** L209
[11] Chen X H, Wu T, Wu G, Liu R H, Chen H and Fang D F 2008 *Nature* **453** 761
[12] Steglich F, Aarts J, Bredl C D, Lieke W, Meschede D, Franz W and Schäfer H1979 *Phys. Rev. Lett.* **43** 1892
[13] Bednorz J G and Müller K A 1986 *Z. Phys. B: Condens. Matter* **64** 189
[14] Gumeniuk R, Schnelle W, Rosner H, Nicklas M, Leithe-Jasper A and Grin Y 2008 *Phys. Rev. Lett.* **100** 017002
[15] Maisuradze A, Nicklas M, Gumeniuk R, Baines C, Schnelle W, Rosner H, Leithe-Jasper A, Grin Y and Khasanov R 2009 *Phys. Rev. Lett.* **103** 147002
[16] Maisuradze A, Schnelle W, Khasanov R, Gumeniuk R, Nicklas M, Rosner H, Leithe-Jasper A, Grin Y, Amato A and Thalmeier P 2010 *Phys. Rev. B* **82** 024524
[17] Maple M B, Henkie Z, Yuhasz W M, Ho P C, Yanagisawa T, Sayles T A, Butch N P, Jeffries J R and Pietraszko A 2007 *J. Magn. Magn. Mater.* **310** 182
[18] Aoki Y, Tsuchiya A, Kanayama T, Saha S R, Sugawara H, Sato H, Higemoto W, Koda A, Ohishi K, Nishiyama K and Kadono R 2003 *Phys. Rev. Lett.* **91** 067003
[19] Tee X Y, Luo H G, Xiang T, Vandervelde D, Salamon M B, Sugawara H, Sato H, Panagopoulos C and Chia E E M2012 *Phys. Rev. B* **86** 064518
[20] Sigrist M and Ueda K 1991 *Rev. Mod. Phys.* **63** 239
[21] Norman M R 2011 *Science* **332** 196
[22] Keller L, White J S, Frontzek M, Babkevich P, Susner M A, Sims Z C, Sefat A S, Rønnow H M and Rüegg C 2015 *Phys. Rev. B* **91** 020409
[23] Kotegawa H, Nakahara S, Akamatsu R, Tou H, Sugawara H and Harima H 2015 *Phys. Rev. Lett.* **114** 117002
[24] Matsuda M, Lin F K, Yu R, Cheng J G, Wu W, Sun J P, Zhang J H, Sun P J, Matsubayashi K, Miyake T, Kato T, Yan J Q, Stone M B, Si Q M, Luo J L and Uwatoko Y 2018 *Phys. Rev. X* **8** 031017
[25] Chandrasekhar B S 1962 *Appl. Phys. Lett.* **1** 7
[26] Clogston A M 1962 *Phys. Rev. Lett.* **9** 266
[27] Shao Y T, Wu X X, Wang L, Shi Y G, Hu J P adn Luo J L 2018 *Europhys. Lett.* **123** 57001
[28] Adroja D T, Bhattacharyya A, Telling M, Feng Yu, Smidman M, Pan B, Zhao J, Hillier A D, Pratt F L and Strydom A M 2015 *Phys. Rev. B* **92** 134505
[29] Zhi H Z, Imai T, Ning F L, Bao J K and Cao G H 2015 *Phys. Rev. Lett.* **114** 147004
[30] Yang J, Tang Z T, Cao G H and Zheng G Q 2015 *Phys. Rev. Lett.* **115** 147002
[31] Luo J, Yang J, Zhou R, Mu Q G, Liu T, Ren Zhi an, Yi C J, Shi Y G and Zheng G Q 2019 *Phys. Rev. Lett.* **123** 047001
[32] Shu L, Higemoto W, Aoki Y, Hillier A D, Ohishi K, Ishida K, Kadono R, Koda A, Bernal O O, MacLaughlin D E, Tunashima Y, Yonezawa Y, Sanada S, Kikuchi D, Sato H, Sugawara H, Ito T U and Maple M B 2011 *Phys. Rev. B* **83** 100504
[33] Sajilesh K P, Singh D, Biswas P K, Hillier A D and Singh R P 2018 *Phys. Rev. B* **98** 214505
[34] Wu W, Liu K, Li Y J, Yu Z H, Wu D S, Shao Y T, Na S H, Li G, Huang R Z, Xiang T and Luo J L 2019 *Natl. Sci. Rev.* **7** 21
[35] Chen C S, Wu Q, Zou M Y, Zhu Z H, Yang Y X, Tan C, Hillier A D, Chang J, Luo J L, Wu W and Shu L 2024 *npj Quantum Mater.* **9** 22
[36] Li Y J, Wu W, Liu K, Yu Z H, Wu D S, Shao Y T, Na S H, Li G, Zheng P and Xiang T and Luo J L 2020 *Europhys. Lett.* **128** 67002
[37] Blundell S J 1999 *Contemp. Phys.* **40** 175
[38] Yaouanc A. and Dalmas de Réotier P 2011 *Muon Spin Rotation, Relaxation, and Resonance: Applications to Condensed Matter* (New York: Oxford University Press)
[39] Amato A 1997 *Rev. Mod. Phys.* **69** 1119
[40] Luke G M, Fudamoto Y, Kojima K M, Larkin M I, Merrin J, Nachumi B, Uemura Y J, Maeno Y, Mao Z Q, Mori H and Nakamura H 1998 *Nature* **394** 558
[41] Hillier A D, Quintanilla J, Mazidian B, Annett J F and Cywinski R 2012 *Phys. Rev. Lett.* **109** 097001
[42] Sonier J E, Brewer J H and Kiefl R F 2000 *Rev. Mod. Phys.* **72** 769
[43] Shu L, MacLaughlin D E, Varma C M, Bernal O O, Ho P C, Fukuda R H, Shen X P and Maple M B 2014 *Phys. Rev. Lett.* **113** 166401
[44] Ding Z F, Zhang J, Tan C, Huang K, Chen Q Y, Lum I, Bernal O O, Ho P C, MacLaughlin D E, Maple M B and Shu L 2019 *Phys. Rev. B* **99** 035136
[45] Suter A and Wojek B M 2012 *Phys. Procedia* **30** 69
[46] Ashcroft N W and Mermin N D 1976 *Solid State Physics* (Harcourt College Publishers) p. 739
[47] Singh D, Sajilesh K P, Marik Sourav, Hillier A D and Singh R P 2019 *Phys. Rev. B* **99** 014516
[48] Shang T, Ghosh S K, Zhao J Z, Chang L J, Baines C, Lee M K, Gawryluk D J, Shi M, Medarde M, Quintanilla J and Shiroka T 2020 *Phys. Rev. B* **102** 020503
[49] Aoki D, Brison J P, Flouquet J, Ishida K, Knebel G, Tokunaga Y and Yanase Y 2022 *J. Phys.: Condens. Matter* **34** 243002
[50] Hardy F, Aoki D, Meingast C, Schweiss P, Burger P, von Löhneysen H and Flouquet J 2011 *Phys. Rev. B* **83** 195107
[51] Reference [38], Appendix A.2
[52] This is a crude approximation. See, e.g., Ref. [38], Chapter 11, for more detail
[53] Sonier J E 2007 *Rep. Prog. Phys.* **70** 1717
[54] Michael T 1975 *Introduction to Superconductivity* 2nd Edn. (McGraw-Hill)
[55] Khasanov R, Conder K, Pomjakushina E, Amato A, Baines C, Bukowski Z, Karpinski J, Katrych S, Klauss H H, Luetkens H, Shengelaya A and Zhigadlo N D 2008 *Phys. Rev. B* **78** 220510
[56] Carrington A and Manzano F 2003 *Physica C* **385** 205
[57] Hillier A D, Quintanilla J and Cywinski R 2009 *Phys. Rev. Lett.* **102** 117007
[58] Luke G M, Keren A, Le L P, Wu W D, Uemura Y J, Bonn D A, Taillefer L and Garrett J D 1993 *Phys. Rev. Lett.* **71** 1466
[59] Uemura Y J, Nishiyama K, Yamazaki T and Nakai R 1981 *Solid State Commun.* **39** 461
[60] Zhang J, Ding Z F, Huang K, Tan C, Hillier A D, Biswas P K, MacLaughlin D E and Shu L 2019 *Phys. Rev. B* **100** 024508
[61] 1988 *Physica Reference Manual* (TRIUMF 4004 Wesbrook Mall, Vancouver, B.C., Canada V6T 2A3)
[62] Broil S and Jeitschko W 1995 *Z. Naturforsch.* **50b** 905
[63] Leggett A J 1975 *Rev. Mod. Phys.* **47** 331
[64] Bouquet F, Wang Y, Fisher R A, Hinks D G, Jorgensen J D, Junod A and Phillips N E 2001 *Europhys. Lett.* **56** 856
[65] Jiao L, Howard S, Ran S, Wang Z, Rodriguez J O, Sigrist M, Wang Z, Butch N P and Madhavan V 2020 *Nature* **579** 523
[66] Ran S, Eckberg C, Ding Q P, Furukawa Y, Metz T, Saha S R, Liu IL, Zic M, Kim H, Paglione J P and Butch N P 2019 *Science* **365** 684
[67] Sugawara H, Kobayashi M, Osaki S, Saha S R, Namiki T, Aoki Y and Sato H 2005 *Phys. Rev. B* **72** 014519